One Earth

Resource

High-resolution land-use maps from 1960 to 2100

Graphical abstract

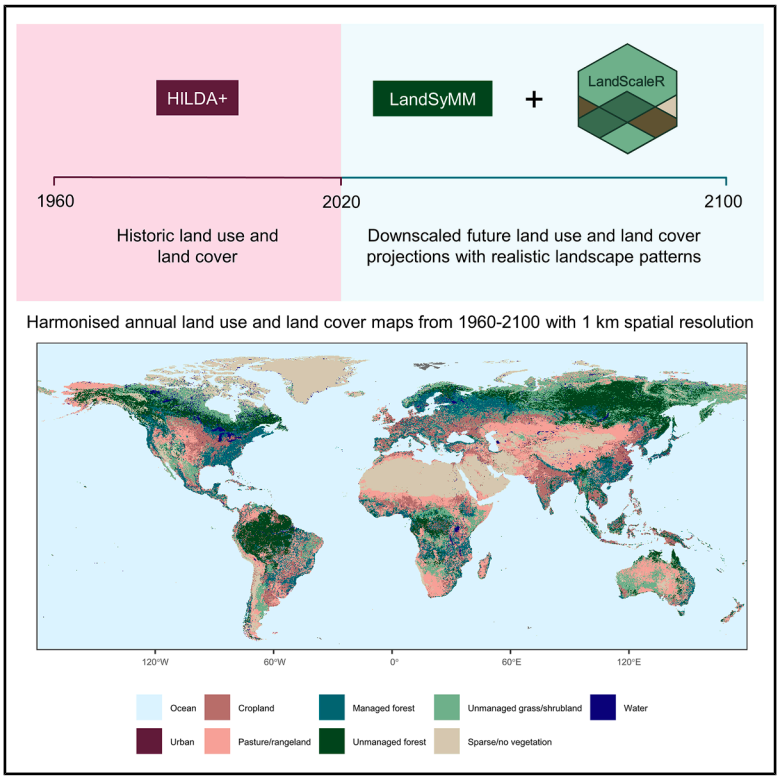

Highlights

- We present harmonized global land-use and land-cover maps for five scenarios
- Dataset spans 1960–2100 with 1 km spatial and yearly temporal resolutions
- Future projections were made by downscaling outputs from a global land-use model
- Downscaling method was calibrated to ensure realistic landscape patterns

Authors

Tamsin L. Woodman, Bartlomiej Arendarczyk, Karina Winkler, ..., David F.R.P. Burslem, Peter Alexander, Justin M.J. Travis

Correspondence

tamsin.woodman@ed.ac.uk

In brief

Harmonized land-use and land-cover datasets that include past and future periods are key to solving sustainability issues, such as climate change and biodiversity loss. However, existing harmonized products do not account for the spatial patterns of future landscapes and have coarse resolutions that do not match the scale at which environmental processes occur. We present a new global-scale, high-resolution dataset of harmonized land-use and land-cover maps for five future scenarios for the period 1960–2100.

Woodman et al., 2026, One Earth 9, 101525
February 20, 2026
https://doi.org/10.1016/j.oneear.2025.101525

CellPress

One Earth

CellPress
OPEN ACCESS

Resource

High-resolution land-use maps from 1960 to 2100

Tamsin L. Woodman,[1,2,8,*] Bartlomiej Arendarczyk,[2] Karina Winkler,[3] Roslyn C. Henry,[1,4] Felix Eigenbrod,[5] David F.R.P. Burslem,[1,4] Peter Alexander,[2,6] and Justin M.J. Travis[1,7]

[1]School of Biological Sciences, University of Aberdeen, Zoology Building, Tillydrone Avenue, Aberdeen AB24 2TZ, UK
[2]School of GeoSciences, University of Edinburgh, Drummond Street, Edinburgh EH8 9XP, UK
[3]Land Use Change and Climate, IMKIFU, Karlsruhe Institute of Technology (KIT), Campus Alpin, Garmisch-Partenkirchen, Germany
[4]Interdisciplinary Institute, University of Aberdeen, UK
[5]School of Geography and Environmental Science, University of Southampton, Highfield Campus, Southampton SO17 1BJ, UK
[6]Global Academy of Agriculture and Food Systems, University of Edinburgh, Edinburgh, Scotland EH25 9RG, UK
[7]Faculty of Forestry, Universitas Gadjah Mada, Jl. Agro No. 1 Bulaksumur, Sleman, Yogyakarta, Indonesia
[8]Lead contact
*Correspondence: tamsin.woodman@ed.ac.uk
https://doi.org/10.1016/j.oneear.2025.101525

SCIENCE FOR SOCIETY Anthropogenic land-use and land-cover change is a major driver of climate change and biodiversity loss. Land-use and land-cover change also leads to changes in the spatial pattern of Earth's landscapes, which have further negative impacts on environmental processes. For example, deforestation can increase the distance between forest patches, making it harder for species to move between them. Harmonized land-use and land-cover datasets contain standardized maps of global land use and land cover through time, without any gaps or sudden changes between historic and future periods. Harmonized datasets are important for addressing the negative consequences of land-use and land-cover change because they are used in environmental models to predict its impacts on processes such as carbon emissions and species movement. However, existing harmonized datasets do not project the spatial pattern of land-use and land-cover change into the future and have coarse resolutions that do not match the fine scales on which environmental processes occur. We present a high-resolution, global-scale harmonized land-use and land-cover dataset for five future scenarios that spans the period 1960–2100. The spatial pattern of land-use and land-cover change was accounted for when generating the future maps to ensure that they have realistic spatial patterns. This new dataset will be suitable for integration with a range of environmental models, such as those that model biodiversity, climate, and fire, and therefore offers an important tool for understanding the effects of land-use and land-cover change and developing solutions to environmental challenges.

SUMMARY

Global-scale land-use and land-cover (LULC) datasets are essential for addressing sustainability challenges, including climate change and biodiversity loss. Existing harmonized LULC products (without discontinuities between past and present) have coarse temporal and spatial resolutions and do not consider landscape patterns, which are important for environmental processes, such as species movement. We present a downscaled global LULC dataset for five future scenarios, with 1 km spatial and yearly temporal resolution, that is harmonized with historic LULC to span the period 1960–2100. Future projections indicate significant landscape change and emphasize the importance of incorporating local-scale processes in global LULC projections. Our harmonized LULC dataset will be advantageous for studying the impacts of LULC change because it was validated to ensure that future LULC projections have realistic landscape patterns, and it has high spatial and temporal resolutions that better match the scale of environmental processes compared to existing products.

INTRODUCTION

Anthropogenic land-use and land-cover (LULC) change poses a major risk to the Earth system, including the processes that maintain the integrity of climate,[1] biodiversity,[2,3] and hydrological[4,5] systems. Approximately 75% of the Earth's surface is already affected by anthropogenic actions,[6,7] and LULC change is predicted to continue in the future to meet demands for food

Please cite this article in press as: Woodman et al., High-resolution land-use maps from 1960 to 2100, One Earth (2025), https://doi.org/10.1016/j.oneear.2025.101525

and energy from a growing human population.[8,9] LULC change also causes the fragmentation of natural ecosystems into smaller patches,[10,11] which can have further negative effects on the Earth system, such as additional carbon emissions from forest edges.[12] An understanding of both historic and future LULC is necessary to investigate and predict the impacts of anthropogenic activities on the environment and to solve key challenges that are facing our societies, such as climate change and food security.[8,13]

The spatial arrangement of LULC classes within a landscape is important for environmental and ecological processes, such as the occurrence and spread of fire,[14,15] hydrological dynamics,[16] and species movement,[17] but future global-scale LULC projections do not explicitly account for the spatial pattern of LULC change. Patterns of landscape change are generated by complex interactions between many factors, including human LULC change, landscape history, topography, and climate, which vary through time and space.[18] Therefore, we would expect that patterns of LULC change will also show spatiotemporal variation.[19] Even within what are considered relatively homogeneous regions, such as Amazonia, there is considerable variation in the spatial pattern of forest fragmentation, driven by factors including land ownership and road access.[20,21] While there are multiple examples of global-scale high-resolution future LULC projections,[22–30] which are produced by downscaling coarse-resolution maps to finer resolutions,[31] none have been validated to ensure accuracy in reproducing the spatial patterns of LULC change across scales. Thus, the lack of global-scale future LULC projections that directly account for variation in the spatial pattern of LULC change represents a major gap with substantial implications for modeling environmental and ecological futures.

A further limitation of existing global-scale downscaled LULC projections is their coarse temporal resolution; the finest resolution of current downscaled LULC projections is 5 years,[23–25] while some only provide a single year of data.[28] Coarse temporal resolution may prevent the integration of downscaled LULC projections with process-based environmental models that use a finer-resolution timestep, such as the biodiversity model RangeShifter.[32]

Global-scale LULC datasets that span both historic and future periods are indispensable for quantifying the environmental impacts of LULC change, but existing products lack the high spatial and temporal resolutions ideally required for modeling environmental and ecological processes.[33,34] Potential discontinuities between historic LULC datasets and future projections, for example, those caused by different spatial resolutions or LULC definitions, give rise to the need for harmonization to ensure a continuous transition from historic LULC to future projections.[35,36] Discontinuities between historic and future periods can generate large amounts of LULC change in model outputs, which may then cause difficulties in understanding the effects of LULC change within ecosystem service models such as the Lund-Potsdam-Jena General Ecosystem Simulator (LPJ-GUESS).[36] One widely used product, the Land-Use Harmonization 2 (LUH2) dataset, provides global LULC data from 850 to 2100 that are harmonized across historical and future periods.[35] While LUH2 has facilitated substantial advances in predicting the impacts of LULC change on environmental and ecological processes,[37–39] it has notable limitations. For example, the coarse spatial resolution of LUH2 (approximately 28 × 28 km at the equator) overlooks the fine-scale spatial patterns critical for modeling ecological and biophysical processes,[33,34] such as species dispersal[40] and carbon emissions.[41] Additionally, LUH2 relies on only a few sources of observational land-cover data to determine historic change and uses different land-use models to make future LULC projections for each scenario,[35] despite previous observations that model differences can cause more variation than scenarios.[42] Overall, there is an opportunity for a new global-scale harmonized LULC product with high spatial and temporal resolutions that considers future landscape patterns and uses a consistent modeling framework to make projections.

Here, we present a set of global-scale future LULC projections with high temporal (yearly) and spatial (0.01°; approximately 1 km at the equator and 0.1 km at 85° latitude) resolutions from 2021 to 2100 that are harmonized with a historic LULC product encompassing the period from 1960 to 2020.[43] The high-resolution future LULC projections were generated by downscaling future LULC projections from the Land System Modular Model (LandSyMM; https://landsymm.earth/)[36] with the spatial downscaling algorithm LandScaleR.[44] LandScaleR uses neighborhood rules and a stochasticity parameter that regulates the probability of each grid cell undergoing LULC change to guide the location of change on a high-resolution reference map, and it has been shown to generate realistic spatial patterns.[44]

Overall, this work addresses crucial gaps in existing global harmonized LULC products. Firstly, we provide a fully consistent harmonized dataset of LULC maps from 1960 to 2100 with a higher spatial resolution than existing products (e.g., 1 × 1 km versus 28 × 28 km in LUH2[35]) that better matches the scale at which environmental and ecological processes operate. Secondly, to our knowledge, this is the first study to account for regional variation in spatial patterns of LULC change through calibration with historic LULC data at both global and country scales, which reflects the influence of factors such as land-use and management practices, topography, and environmental conditions.[18] Our explicit consideration of spatial patterns during downscaling enables a more realistic representation of landscape structure in future LULC projections, which will be important for modeling the impacts of LULC change on environmental processes. Thirdly, the same modeling framework was used to generate the future LULC projections, thereby removing variation caused by the use of different land-use models.[42] Finally, our future LULC projections have improved temporal resolution compared to current global-scale downscaled future projections, which, at best, produce maps at 5 yearly intervals.[23–25] We anticipate that our dataset will facilitate the integration of LULC change with a wide range of environmental and ecological models, such as climate, biodiversity, fire, and hydrology. Therefore, our harmonized product provides a strong foundation for understanding how anthropogenic LULC change impacts the natural environment, offering a transformative tool for developing solutions to sustainability challenges, such as biodiversity loss and climate change.

Please cite this article in press as: Woodman et al., High-resolution land-use maps from 1960 to 2100, One Earth (2025), https://doi.org/10.1016/j.oneear.2025.101525

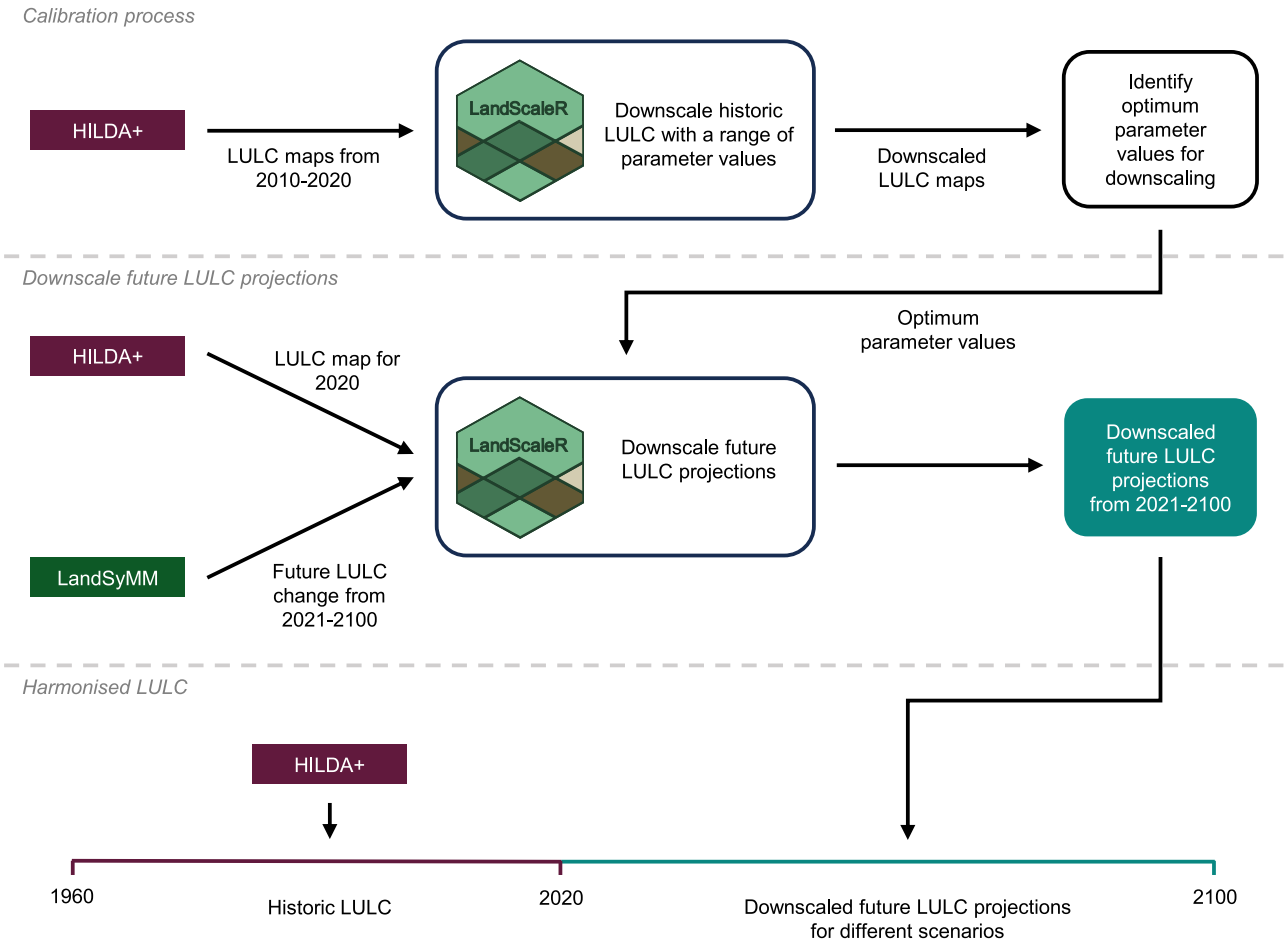

Figure 1. Overview of the downscaling process used to generate high-resolution future land-use and land-cover projections

Historic land-use and land-cover (LULC) maps from HILDA+ between 2010 and 2020 were used to identify the optimum parameters for downscaling with the LandScaleR algorithm.[44] The optimum parameter values were used to downscale global-scale future LULC change projections from the LandSyMM modeling framework[36] for a range of socioeconomic and climate scenarios.[48–51] Downscaled future LULC projections with 0.01° spatial resolution (approximately 1 × 1 km at the equator) and yearly temporal resolution from 2021 to 2100 were generated. These downscaled LULC projections can be combined with HILDA+, which spans the period from 1960 to 2020, to give harmonized LULC maps from 1960 to 2100 with consistent spatial and temporal resolutions.

RESULTS

Method summary

We downscaled future LULC change projections using the LandScaleR algorithm,[44] which converts coarse-resolution LULC change projections into high-resolution ones using a fine-resolution reference map, neighborhood rules, and a stochasticity parameter (*f* value) that controls the likelihood that each grid cell will be converted to a new LULC class. The *f* value introduces stochasticity into the placement of new LULC on the reference map and allows for the appearance of new LULC patches in a landscape, so it is important for generating realistic landscape patterns.[44] Lower values of *f* lead to fewer LULC patches that are more highly aggregated, while higher values generate more, less-aggregated LULC patches.

LandScaleR was calibrated for downscaling future LULC projections using historic data from the HILDA+ LULC reconstruction[43] between 2010 and 2020 (Figure 1) to select the *f* values that best recreated historic LULC change in terms of both grid-cell-level changes and landscape patterns. Landscape patterns are driven by multiple interacting natural and anthropogenic variables,[18] so we expected that historic LULC change may have generated different landscape patterns across countries. We therefore calibrated LandScaleR to find the optimum *f* values for downscaling future LULC projections at both the country scale, where one optimum *f* value was identified per country group, and at the global scale, where a single optimum *f* value was chosen based on the global average downscaling error (DE). To select the optimum *f* values for downscaling, we used a combined error metric that accounted for accuracy at both the grid-cell and landscape levels, based on the Figure of Merit[45,46] and landscape metrics,[47] respectively.

The optimal *f* values identified during the calibration process were used to downscale future LULC projections from LandSyMM[36] from 0.5° to 0.01° (approximately 55 × 55 km to 1 × 1 km at the equator) for the years 2021–2100. LandSyMM is a state-of-the-art global-scale land system model that couples the parsimonious land-use model[52] (PLUM) to the LPJ-GUESS

Please cite this article in press as: Woodman et al., High-resolution land-use maps from 1960 to 2100, One Earth (2025), https://doi.org/10.1016/j.oneear.2025.101525

vegetation model.[36,53] PLUM is a global-scale land-use model that uses scenarios of socioeconomic development and detailed crop yield projections from LPJ-GUESS to project future LULC.[52] LandSyMM is a unique land system model because it uses highly detailed representations of crop yields and agricultural inputs and does not assume that markets are in equilibrium every year. Moreover, the optimization of land use occurs at a much higher resolution in LandSyMM compared to similar models.[36] Outputs from LandSyMM have a spatial resolution of 0.5° compared to regional outputs from models such as GCAM and MAGNET,[52] which should help to reduce uncertainty during downscaling. A detailed description of the calibration and downscaling procedures is given in the methods section.

Resource description

We provide a set of global-scale downscaled future LULC projections with yearly temporal and 0.01° spatial resolution covering the time period 2021 to 2100. The LandSyMM model can generate future LULC projections under a variety of climatic and socioeconomic development scenarios.[36] We chose to downscale LULC projections for the five SSP scenarios, which are narratives of possible future socioeconomic changes, and a likely representative concentration pathway (RCP), which details expected atmospheric concentrations and climate outcomes, for each scenario.[48–51] The five scenarios were SSP1-RCP2.6, which assumes that sustainable development limits climate change; SSP2-RCP4.5, the "middle-of-road" scenario where development continues as it has historically; SSP3-RCP7.0, the "regional rivalry" scenario where increased nationalism and attention to regional concerns lead to difficulties with mitigations and adaptations to climate change; SSP4-RCP6.0, which assumes increasing inequality within and between countries; and SSP5-RCP8.5, with rapid development fueled by dependence on fossil fuels, which drives climate change.[48–50] We provide two alternative global downscaled maps for each scenario: one that uses the country-scale optimum *f* values from the calibration process and a second that applies the global-scale optimum *f* value.

LULC from HILDA+ v.2b[43] in 2020 was used as the reference map for downscaling to ensure that the downscaled future LULC projections were harmonized with a historic LULC dataset. Combining HILDA+ and the future downscaled LULC projections produces a harmonized LULC product spanning the period from 1960 to 2100 with consistent spatial and temporal resolution. The harmonized LULC product has nine LULC classes: ocean, urban, cropland, pasture/rangeland, managed forest, unmanaged forest, unmanaged grass/shrubland, sparse/no vegetation, and water.

Technical validation

Variation in the spatial pattern of recent LULC change

The calibration process highlighted substantial differences in the spatial pattern of LULC change between countries over the past decade. Our global map of *f* values (Figure 2) demonstrates how spatially variable patterns of LULC change were over the last decade, with the optimum *f* value ranging from 0.50 to 3.00. As well as calculating the optimum *f* values for each country, we calculated the globally optimal *f* value, which was 1.75 (Figure S1); only 40 out of 164 countries shared the global optimum value. For those countries that deviated considerably from the globally optimum *f* value, using the country-specific value would more accurately reproduce the number and size of patches generated by past LULC change. For example, for Brazil, an *f* value of 1.75 generated 14% more error than the optimum *f* value of 2.50. Using a very low *f* value of 0.50 generated 45% more error than that of the optimum *f* value, resulting in highly aggregated landscape spatial patterns compared to those observed historically (Figure 2C). There were no clear spatial patterns in the optimum *f* value for each country or distinct relationships between the optimum *f* value and country area, area of LULC change per year, or area of each LULC class in 2010 (Figure S2). There was some evidence of temporal changes in the spatial pattern of LULC from 2010 to 2020 at the country scale (for example, in Albania and South Korea; Figure S3), but we found no major evidence for temporal changes in average landscape patterns at the global scale over this decade (Figure S1).

Accounting for spatial patterns in downscaling land-use futures

The change in LULC areas at the global scale, which was driven by the LULC change data from LandSyMM,[36] differed across the five downscaled scenarios (Figures S4–S6). For example, cropland increased most under SSP3-RCP7.0 (+372 Mha between 2021 and 2100), followed by SSP5-RCP8.5 (+235 Mha), but decreased by −25 Mha in SSP1-RCP2.6. Unmanaged forest cover decreased the most by 2100 under SSP3-RCP7.0, with much of this decrease occurring in tropical regions (Figure 3). Large areas of unmanaged forest cover are also predicted to be lost from tropical regions by 2100 under SSP4-RCP6.0, whereas the majority of unmanaged forest cover in tropical regions is expected to remain stable between 2020 and 2100 under scenario SSP1-RCP2.6. Small gains in unmanaged forest cover are projected in boreal regions in SSP1-RCP2.6, SSP3-RCP7.0, and SSP4-RCP6.0, particularly in Canada and Finland. Overall, the amount of LULC change in our downscaled maps matched the projected change from LandSyMM, although there was a very small amount of projected LULC change from LandSyMM (order of magnitude of 0.01% of the total area included in the downscaling simulation; Figure S7) that LandScaleR was unable to allocate to a reference map during the downscaling process due to differences in the distribution of LULC between LandSyMM and HILDA+ in 2020.

Our downscaled maps of LULC futures account for the spatial pattern of LULC change and have a much higher spatial resolution compared to outputs from the LandSyMM model[36] (Figure 4). LandSyMM outputs are fractional and provide the area of each LULC class per 0.5° grid cell, whereas our downscaled maps are categorical and contain a single LULC class for each 0.01° (approximately 1 × 1 km at the equator) grid cell. The high-resolution LULC maps for future scenarios provide ideal inputs for environmental and ecological models.

The choice (country or global scale) of *f* value used for downscaling with LandScaleR can make a considerable and visible difference to the landscape patterns of downscaled maps (Figure 5). For example, using the optimum country-scale *f* value for Papua New Guinea (f = 2.50) generated much less aggregated spatial patterns of LULC compared to using the global-scale optimum *f* value of 1.75. The mean area of LULC patches

Please cite this article in press as: Woodman et al., High-resolution land-use maps from 1960 to 2100, One Earth (2025), https://doi.org/10.1016/j.oneear.2025.101525

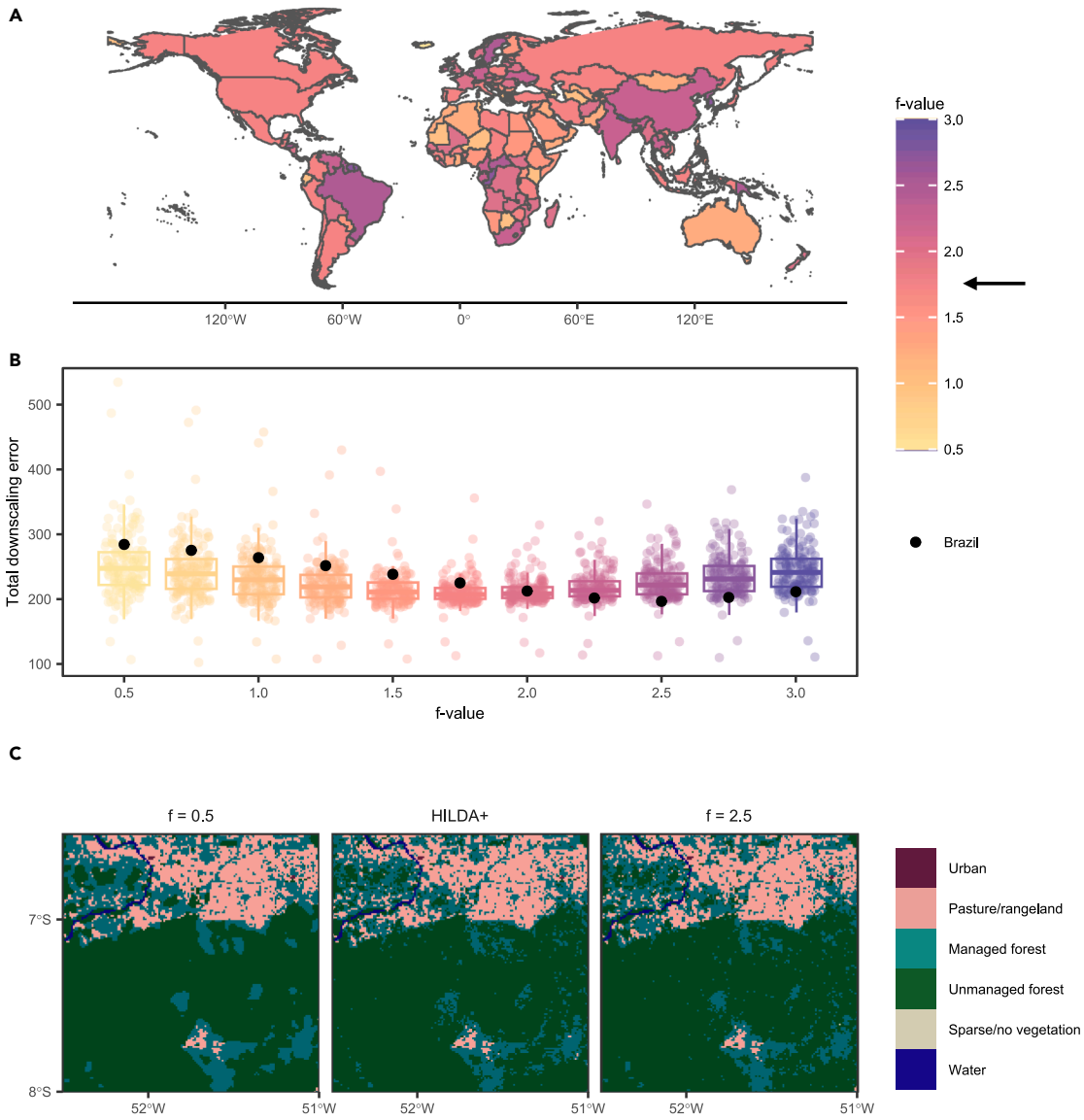

Figure 2. Country-scale variation in spatial patterns of land-use and land-cover change between 2010 and 2020

(A) Optimum *f* value over time for downscaling each country between 2010 and 2020, (B) total downscaling error from 2010 to 2020, and (C) comparison of observed spatial patterns in 2020 (HILDA+) and patterns generated by downscaling with $f = 0.5$ versus $f = 2.5$ for a region of Brazil. The *f* value with the lowest total downscaling error for a country or the globe was selected as the optimum. The total downscaling error was the sum of a combined error metric across all years from 2010 to 2020. The minimum possible total downscaling error was 0, and the maximum was 1,000, with lower values indicating higher accuracy. The global-scale optimum *f* value was 1.75, indicated by an arrow in (A). Boxplots in (B) summarize global-scale total downscaling error from 2010 to 2020, and points are the mean total downscaling error for individual countries across ten replicates. Black points indicate the mean total downscaling error for Brazil, which had an optimum *f* value of 2.5.

in Papua New Guinea was lower and the number of patches (NP) higher when using the country- versus global-scale optimum *f* value to downscale future LULC change under scenarios SSP1-RCP2.6 and SSP4-RCP6.0. Figure 5C demonstrates the impact of the choice of *f* value on a region of Papua New Guinea; unmanaged forest cover is much more fragmented in this region when using the country-scale optimum *f* value rather than the global-scale optimum, which will have implications for modeling environmental and ecological processes that are affected by the spatial pattern of LULC within a landscape. While the choice of *f* value can have a sizable impact on the future patterns of LULC within a country, at the global scale, there is very little difference in average landscape patterns when downscaling is performed using country-scale compared to global-scale parameterization (Figure S8).

Limitations

The harmonized LULC product described here will be advantageous for investigating the effects of future LULC change because it has high spatial and temporal resolutions, and the

Please cite this article in press as: Woodman et al., High-resolution land-use maps from 1960 to 2100, One Earth (2025), https://doi.org/10.1016/j.oneear.2025.101525

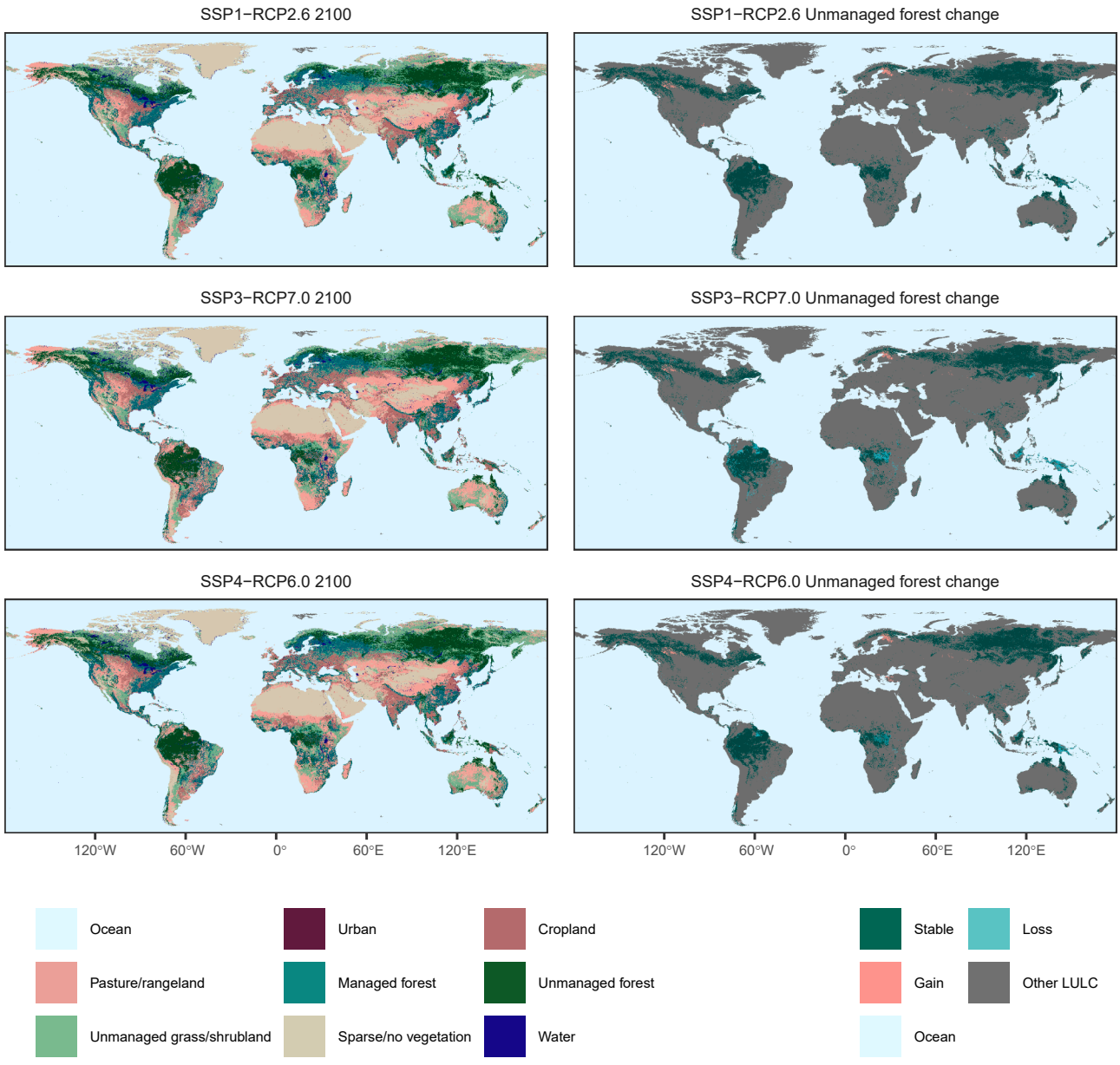

Figure 3. Future projections of global land use and land cover

Future land-use and land-cover (LULC) projections for 2100 with 0.01° resolution (approximately 1 km at the equator) are shown on the left for three scenarios: SSP1-RCP2.6, SSP3-RCP7.0, and SSP4-RCP6.0. The change in unmanaged forest cover from 2020 to 2100 for each of the three scenarios is shown on the right as an example of expected future LULC change. Each of the unmanaged forest-change maps shows the area of unmanaged forest cover that was stable (green), lost (blue), or gained (pink) in 2100 compared to 2020. Gray shading in the plots of LULC in 2100 indicates Svalbard, which is classified as "no data" in HILDA+ and the future LULC projections. Future LULC maps were generated by downscaling 0.5°-resolution LULC projections from LandSyMM[36] to 0.01°. To improve plot readability, only 1,001,300 out of 540,000,000 grid cells were plotted for each global map. Larger versions of global LULC maps in 2100 are provided in Figures S5 and S6.

calibration process ensured that the future LULC projections have realistic landscape patterns. While the spatial patterns in our downscaled future LULC projections are dependent on the *f* value, which is context, location, and time specific, our data offer both country- and global-scale parameterizations, allowing users to select the one that is most appropriate for their location and timescale of interest. In locations where the country- and global-scale optimum *f* values differ, our alternative parameterizations will enable comparisons of the effect of different spatial patterns of future LULC change on environmental and ecological processes. The downscaled LULC projections that used country-scale *f* values will likely be more accurate for studying the effects of LULC over the next few decades. It is currently unclear how the drivers of spatial patterns of LULC change, and therefore the optimum *f* value, will change over longer time periods (Figure S3), so we expect that the downscaled LULC projections generated with

Please cite this article in press as: Woodman et al., High-resolution land-use maps from 1960 to 2100, One Earth (2025), https://doi.org/10.1016/j.oneear.2025.101525

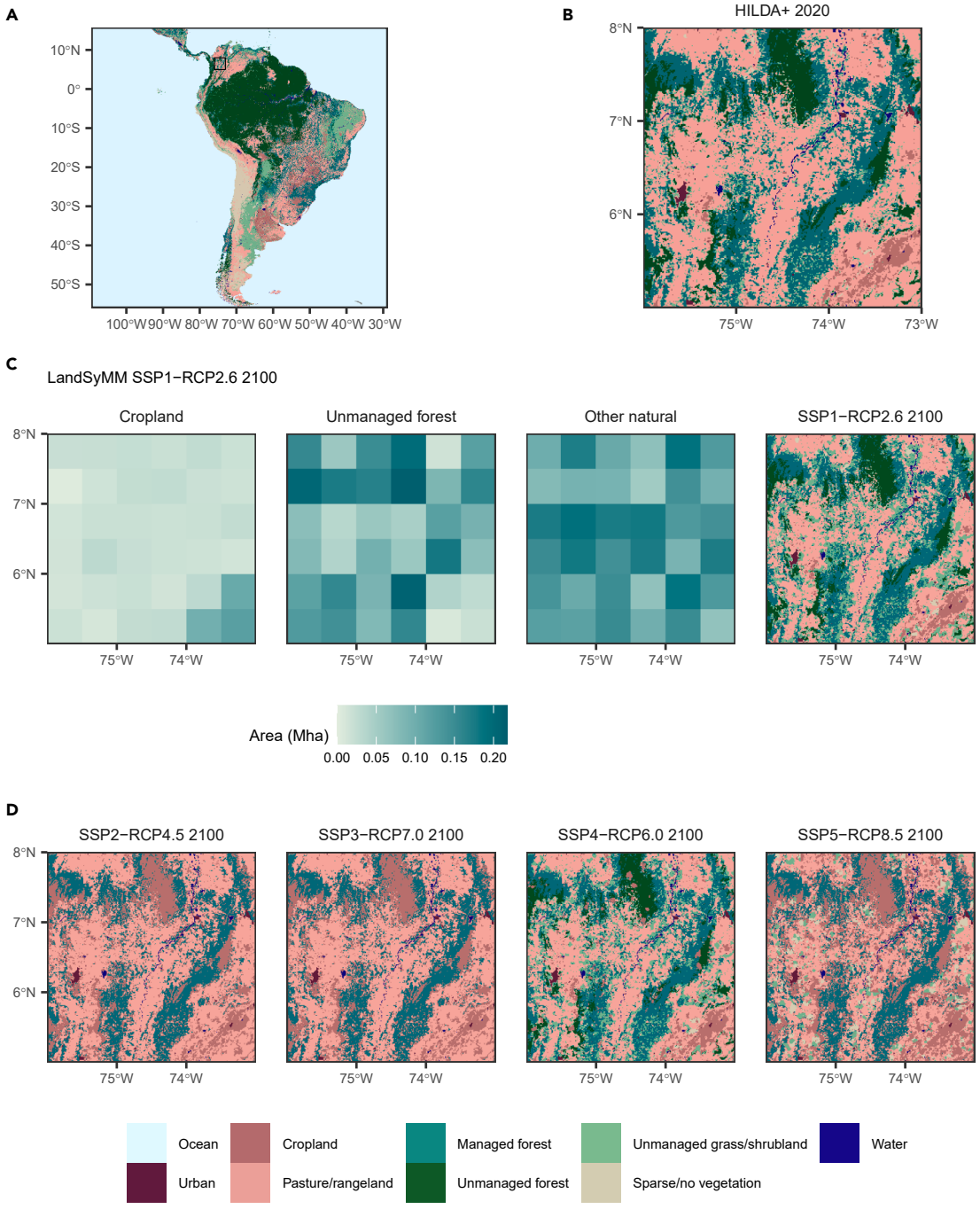

Figure 4. Case study of downscaled land use and land cover projections for Colombia

(A) Land use and land cover (LULC) in South America in 2020 from HILDA+ with a black box to show the expanded region in (B), (C), and (D).

(B) HILDA+ LULC map in 2020 for the expanded region of Colombia.

(C) LULC projections from LandSyMM[36] and the corresponding downscaled map in 2100 for SSP1-RCP2.6.

(D) Downscaled LULC for the region in 2100 for SSP2-RCP4.5, SSP3-RCP7.0, SSP4-RCP6.0, and SSP5-RCP8.5.

Only three example LULC classes from LandSyMM are shown in (C). The other natural LULC class in LandSyMM corresponds to the unmanaged grass/shrubland and sparse/no vegetation classes in the downscaled maps. LandSyMM was not constrained to match the total area of LULC classes in HILDA+ in 2020, so there may be differences in the total area of each LULC class between the LandSyMM and downscaled projections in (C).

a global-scale *f* value may be more applicable for investigating the impacts of LULC change over longer timescales. Future research into the drivers of spatial patterns of LULC change could allow for the *f* value to vary through time and space according to the underlying drivers of change. The downscaled future LULC projections include changes in six LULC classes (cropland,

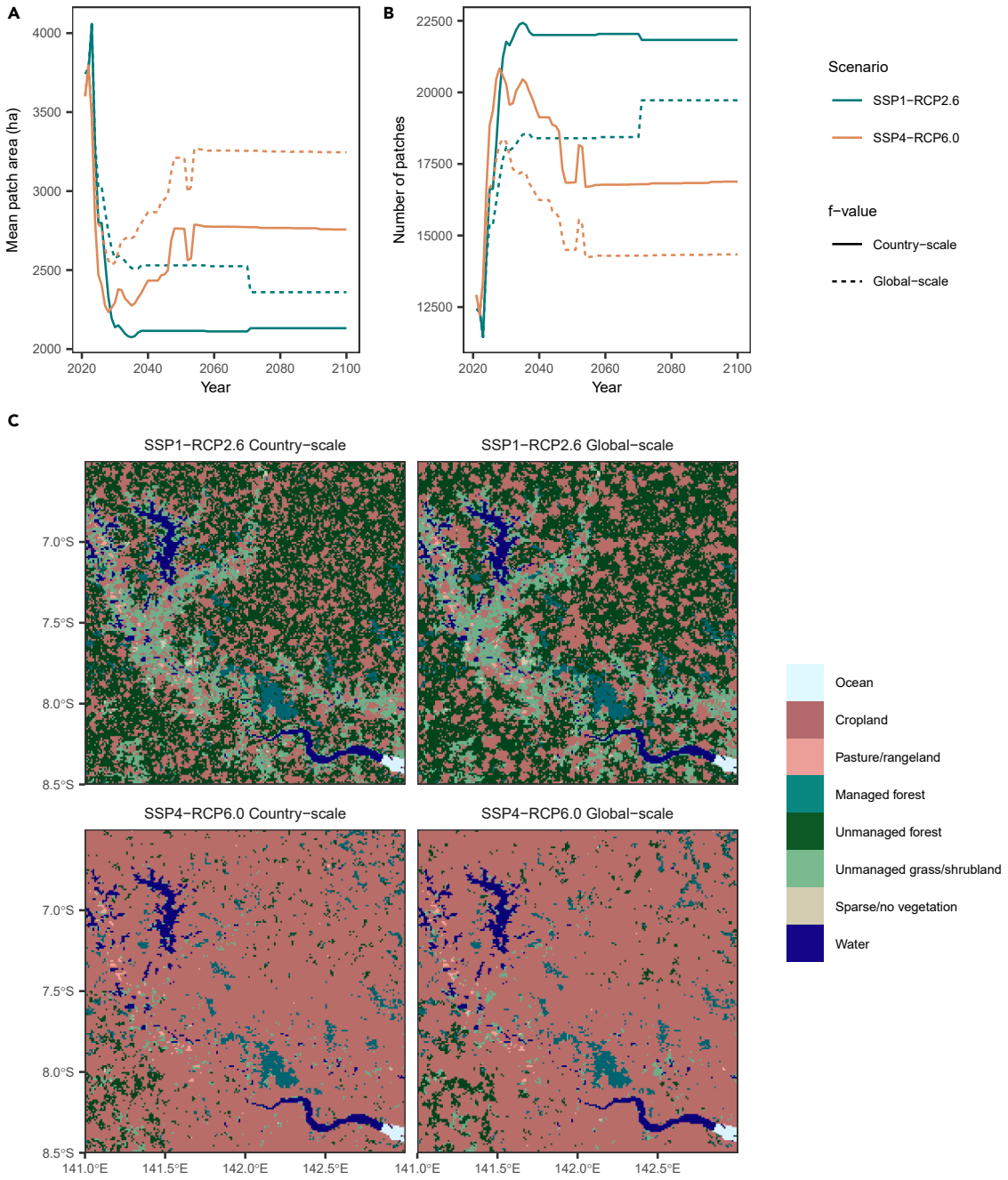

Figure 5. Future landscape patterns vary when downscaling is parameterized at a country versus a global scale

(A) Mean patch area (hectares) across Papua New Guinea between 2021 and 2100.

(B) Total number of patches across Papua New Guinea from 2021 to 2100.

(C) Downscaled future land use and land cover (LULC) in 2100 for a region of Papua New Guinea under two future scenarios generated using country-scale versus global-scale parameterization.

Blue lines in (A) indicate scenario SSP1-RCP2.6, and orange lines indicate scenario SSP4-RCP6.0. Solid lines in (A) represent downscaling with the country-scale optimum *f* value for Papua New Guinea (*f* = 2.50), and dashed lines represent downscaling with the global-scale optimum *f* value (*f* = 1.75).

pasture/rangeland, managed forest, unmanaged forest, unmanaged grass/shrubland, and sparse/no vegetation) and are advantageous compared to existing products that do not distinguish between managed and unmanaged grasslands and forests.[23–25,27–30] Urban LULC is static in our downscaled future projections, as LandSyMM does not currently model changes in urban extent, although only 0.76% of the global land area was urban in 2020. To address this, our future LULC projections could be combined with existing projections of urban LULC,[54] or urban LULC could be modeled in LandSyMM.

Please cite this article in press as: Woodman et al., High-resolution land-use maps from 1960 to 2100, One Earth (2025), https://doi.org/10.1016/j.oneear.2025.101525

DISCUSSION

This study presents a new harmonized global LULC product that spans the period from 1960 to 2100 at approximately 1 × 1 km spatial resolution for five scenarios of socioeconomic development and climate change. Our product addresses key limitations of existing downscaled future LULC projections and harmonized products, such as LUH2.[35] Compared to LUH2, our harmonized product has a much higher spatial resolution (approximately 1 × 1 km versus 28 × 28 km[35]) and thus better matches the scale on which land use affects environmental processes, such as the spatial dynamics of biodiversity loss[33,34] and carbon emissions.[41] The future scenarios in our harmonized LULC product were all generated using the same land system and downscaling models, which reduces model uncertainty compared to LUH2, where a different land-use model is used for each socioeconomic scenario.[35] In contrast to existing high-resolution future LULC projections,[22–24,26–30] our product is harmonized with a temporally extensive historic LULC reconstruction[43] from 1960 to 2020, has higher temporal resolution (yearly versus 5 yearly at best[23–25]), and was calibrated to generate more realistic landscape patterns.

Regional variation in the spatial pattern of LULC change

Our analysis highlights spatiotemporal differences in the spatial patterns of LULC change, which suggests that patterns of LULC change are driven by regionally or locally specific factors, such as climate, topography, and landscape history,[18] that may vary through time. We found no evidence that the spatial pattern of LULC change (as measured by the *f* value in LandScaleR[44]) was driven by the overall area of a country, the amount of LULC change that occurred per year, or the area of LULC classes at the start of the calibration period (Figure S2). Landscape patterns are caused by a wide range of natural and anthropogenic factors,[18,20] including the presence of specific LULC classes,[55] so further research should investigate how the spatial pattern of fine-scale LULC change is related to socioeconomic and environmental variables, such as climate, topography, land use, and gross domestic product (GDP). Population density and the Human Development Index (HDI) have previously been found to be weakly associated with fragmentation of landscape patches within countries,[56] indicating that there may be socioeconomic factors underlying spatial patterns of LULC change and therefore the optimum *f* value for downscaling with LandScaleR. An increased understanding of the factors driving country- and local-scale patterns of LULC change would enable algorithms for projecting fine-scale LULC change to account for the spatiotemporal environmental and socioeconomic characteristics of a region rather than assuming that spatial processes are constant through space and time.

Global versus local approaches to LULC modeling

At the global scale, there was little difference in the average spatial pattern of landscapes when future scenarios were downscaled using country- versus global-scale *f* values (Figure S8); for example, the largest difference in landscape patterns was for SSP5-RCP8.5, where the use of country-scale *f* values increased the mean patch area (AREA_MN) by 1.64% compared to using global-scale *f* values. However, more locally, for example, at the country scale, there can be differences in landscape patterns where the country-scale optimum *f* value differs from the global-scale optimal value that could be material to ecosystem functioning. For example, across Papua New Guinea, there were fewer, smaller patches of LULC when future LULC change scenarios were downscaled with the country-scale optimum *f* value of 2.50 compared to the global-scale optimum *f* value, and these differences were visible across multiple future scenarios (Figure 5). The spatial pattern of LULC change has implications for projecting the future impacts of LULC change on environmental and ecological processes. For instance, more fragmented landscapes tend to have smaller patches of natural habitat that support fewer species,[17,57] while increased isolation of habitat patches can lead to the reduced movement of individuals between patches.[10,58] Thus, using future LULC projections that were downscaled with the country-scale optimum *f* value for Papua New Guinea, which demonstrated increased fragmentation of LULC patches, might suggest that intra-species connectivity and species richness will be lower in the future compared to using LULC projections that were generated with the global-scale *f* value.

Given that spatial patterns are increasingly recognized as important for the accurate modeling of environmental and ecological processes, it is key that we consider carefully how landscape patterns are incorporated into future LULC projections. Our harmonized LULC product will allow future users to select downscaled LULC projections that use country- or global-scale parameterizations. The contrasting spatial patterns between future LULC maps that were downscaled using country- versus global-scale *f* values highlight the importance of integrating local-scale variation in LULC dynamics into global-scale models of LULC change and its impacts.

Relevance for environmental and ecological modeling

The mismatch between the resolution of global-scale land-use models and the scale of environmental processes has historically presented a challenge for integrating global LULC projections with environmental and ecological models,[33,34] particularly process-based models. Our new harmonized dataset aims to overcome this limitation by providing global LULC projections at 1 km resolution with a yearly timestep, which will enable better integration with process-based models. For example, our harmonized dataset could be integrated with the hydrological soil and water assessment tool (SWAT) and SWAT+ models[59,60] to enable the development of hydrological models over large spatial extents[61] and future scenarios. LULC change and landscape patterns are also key for the likelihood of fire occurrence and intensity[14,62,63]; hence, the harmonized dataset developed here will have applications for predicting the future risk of fire ignition, intensity, and spread using well-established models, such as FARSITE and Burn-P3.[64,65] Our harmonized LULC dataset will also be applicable for use in ecosystem service models, such as InVEST, that require spatially explicit LULC data.[66,67] Similarly, process-based ecological models that forecast biodiversity futures under alternative climate, LULC, and management scenarios[32,68,69] will benefit substantially from the availability of our harmonized dataset, as key ecological processes, including dispersal, operate at fine scales that match the resolution of this LULC dataset.

Please cite this article in press as: Woodman et al., High-resolution land-use maps from 1960 to 2100, One Earth (2025), https://doi.org/10.1016/j.oneear.2025.101525

Implications for policymaking and governance

The harmonized, high-resolution LULC product developed in this study has significant implications for investigating the impacts of LULC change on the natural environment, offering important insights for policymakers. By spanning both historic and future periods with consistently high spatial and temporal resolution, our dataset will enable more accurate assessments of the effects of LULC change on environmental and ecological processes and therefore facilitate the development of solutions to challenges such as biodiversity conservation, climate change, and food security.[8,13] Furthermore, our harmonized LULC dataset offers insights into the spatiotemporal heterogeneity of LULC change and could be used to inform spatial planning and adaptive policy design at different scales. Our results indicate that there will be substantial variation in the patterns of future LULC change at local to regional scales, emphasizing the importance of incorporating local-scale processes within global-scale models of LULC change. The variation in historic and future patterns of LULC change observed here highlights that policy interventions will need to be tailored to local conditions rather than relying on global "one-size-fits-all" strategies.

METHODS

Global maps of historic LULC change

We obtained global-scale maps of yearly LULC change from HILDA+ v.2b, which is a reconstruction of global yearly LULC states and transitions at 0.01° spatial resolution.[43,70,71] HILDA+ v.2b was produced using multiple sources of LULC data, in addition to US Food and Agriculture Organization (FAO) statistics, to reconstruct net and gross LULC change on a yearly basis from 1960 to 2020. HILDA+ v.2b has eight LULC classes: ocean, urban, cropland, pasture/rangeland, forest, unmanaged grass/shrubland, sparse/no vegetation, and water. A global classification of the forest LULC class into managed and unmanaged areas is also provided as a separate file in HILDA+ v.2b. We incorporated the global forest management classification into HILDA+ LULC maps to create a set of maps from 1960 to 2020 with the "forest" LULC class replaced by either "managed forest" or "unmanaged forest." A subset of these maps from 2010 to 2020 was then aggregated to 0.5° (approximately 55 × 55 km at the equator) to generate the fraction of each LULC class per grid cell. Yearly LULC change was calculated by subtracting LULC fractions in each year from those in the previous year, creating a set of global-scale yearly maps of LULC change at the same resolution as future LULC projections from the LandSyMM model[36] (0.5°). The "ocean" LULC class was removed from the resulting LULC change maps, which were then used to calibrate LandScaleR. All maps were processed in R v.4.0.0 or v.4.1.3[72] using the "terra" R package v.1.7-23.[73]

Calibration of LandScaleR using historic LULC data

The LandScaleR downscaling algorithm has two parameters that can be tuned by the user to control the level of spatial aggregation in the output maps: the *f* value and the kernel density radius. Increasing the *f* value up to an optimum value facilitates the creation of new LULC patches during downscaling and has been shown to generate realistic landscape patterns.[44] We calibrated the *f* value using historic LULC data from HILDA+ between 2010 and 2020 at both the global and country scales. The kernel density radius sets the number of neighboring grid cells that are used to calculate the kernel density value for each LULC class and focal grid cell; higher kernel density values indicate that a cell is near existing LULC of the same class and therefore more likely to be allocated new LULC. A kernel density radius of 1 specifies that nine first-neighbor grid cells will be used in the calculation of the kernel density value for each focal grid cell. Previous testing showed that setting the kernel density radius to values higher than 1 generated extremely aggregated landscape patterns with fewer, larger patches than those observed in HILDA+ data for Colombia,[44] so we set the kernel density radius to 1 for all downscaling simulations.

The downscaling process was performed separately for 164 country groupings when calibrating LandScaleR due to computational limitations, and the country-scale downscaled maps were merged to create global downscaled products. The groupings were defined using country-group definitions from the PLUM sub-model of LandSyMM,[36,52] which models global food demand, trade, and land-use change. Some small countries are combined in PLUM to reduce computational requirements during the modeling process. We only calibrated LandScaleR for countries that are included in the PLUM land-use optimization process and can therefore undergo LULC change in the future projections. Also, note that we divided the "France" country grouping into three: "France," "French Guiana," and "Réunion." Three countries that cross the international date line (New Zealand, the US, and Russia) were each divided into their separate territories on either side of it to reduce computational requirements. A map of countries from the Database of Global Administrative Boundaries (GADM) dataset v.3.6,[74] downloaded via the "geodata" R package v.0.5-9[75] on February 27, 2024, was used to ensure that 0.5°-resolution HILDA+ grid cells were matched to the relevant country group from PLUM.

Yearly 0.5°-resolution maps of LULC change derived from HILDA+ between 2010 and 2020 were downscaled to 0.01° spatial resolution multiple times with different *f* values to calibrate LandScaleR. Previous work found that the optimum *f* value for downscaling historic LULC change in Colombia was 2.0,[44] so we ran an initial round of calibration for each country group using five *f* values from 1.0 to 5.0 with an interval of 1.0 to narrow down the possible parameter space. Given that LandScaleR is stochastic, ten repeats were run for each *f* value during calibration, and the average accuracy across these repeats was used to determine the optimum *f* value. The output discrete country-scale downscaled maps were merged to generate global downscaled maps at 0.01° resolution from 2010 to 2020, and the accuracy of the downscaled maps compared to the actual HILDA+ maps was calculated. The initial round of calibration demonstrated that the optimum *f* value for each country varied between 1.0 and 3.0, so a second round of calibration was run with ten more values of *f* (0.5, 0.75, 1.25, 1.5, 1.75, 2.25, 2.5, 2.75, 3.25, and 3.5). HILDA+ LULC in 2010 was used as the reference map for downscaling, and each LULC class in the reference map was matched to itself in the LULC change maps. Note that the optimum *f* value appeared to vary through time for some countries, but temporal variation in the optimum *f* value was not considered during calibration, as we aimed to select the *f* value that minimized error over time. All downscaling simulations were

run using LandScaleR v.1.1.0[44] on a high-performance computer with R v.4.1.3[72] and terra v.1.7-23.[73]

Validation of LandScaleR and selection of optimum *f* value

To validate the accuracy of LandScaleR and choose the optimum *f* value for downscaling future LULC projections, we calculated five landscape metrics and the Figure of Merit. Landscape metrics were used to test whether LandScaleR generated realistic landscape patterns compared to observed patterns in HILDA+. Five metrics were chosen that have previously been used to validate LandScaleR: class area (CA), which is the total area of each LULC class in the landscape; AREA_MN (ha); NP; aggregation index (AI), which is a measure of LULC aggregation; and edge density (ED; m ha^{-1}), which is the total length of edges in a landscape standardized by landscape area.[44] The AI is calculated by summing the number of edges shared by grid cells of the same LULC class and then dividing by the hypothetical number of edges that would be shared between the same cells if the landscape were aggregated as much as possible.[47] The "landscapemetrics" R package v.2.1.1[47] was used to calculate landscape metrics.

We generated landscape metrics for each year in the calibration period for both the reference HILDA+ and downscaled maps for each country. Note that each country map was reprojected to the Eckert IV projection prior to calculating country-level landscape metrics.[44] Landscape metrics were not calculated at a global scale, as there was potential for distortion to occur when reprojecting global maps from WGS84 to Eckert IV, which could alter the landscape patterns. After calculating landscape metrics, the relative error (RE) was used to compare the reference and downscaled landscape metrics and assess how well LandScaleR was able to recreate the observed landscape patterns in HILDA+. The RE was calculated for each year and landscape metric as in Dezhkam et al.[76]:

$$RE_M = \frac{M_L - M_H}{M_H} \times 100, \quad \text{(Equation 1)}$$

where M_L indicates landscape metrics from downscaled maps and M_H indicates observed metrics from HILDA+.

Figure of Merit was used to measure the overlap between the change predicted by LandScaleR during downscaling and the change observed in HILDA+[45,46] and was chosen as a grid-cell-level measure of downscaling accuracy. Figure of Merit was calculated as done previously for Colombia[44]:

$$FoM = \frac{B}{A+B+C+D} \times 100, \quad \text{(Equation 2)}$$

where *A* is the number of grid cells that were observed to change LULC class in HILDA+ but were not predicted to change by LandScaleR; *B* is the number of grid cells that changed in both HILDA+ and the downscaled maps and the LULC class was correctly predicted by LandScaleR; *C* is the number of grid cells that changed in both the HILDA+ and downscaled maps but were incorrectly predicted by LandScaleR; and *D* is the number of grid cells that were predicted to change by LandScaleR but were not observed to change in HILDA+. The values for Figure of Merit range from 0% to 100%, with 0% meaning no change was allocated correctly and 100% meaning all change was correctly placed. Figure of Merit was calculated on a yearly basis, as well as across the entire calibration period (from 2010 to 2020), at both the country and global scales.

A single metric of DE was computed for each year in every downscaling replicate to assess the performance of LandScaleR when using different *f* values. DE was calculated by combining yearly Figure of Merit and RE of landscape metrics into a "fitness function," similar to those used by past studies to calibrate cellular automata land-use models.[77,78] The DE metric was calculated using the equation

$$DE = w_{FoM} \times (100 - FoM) + w_L \times \frac{\sum_{M=1}^{4} RE_M}{4}, \quad \text{(Equation 3)}$$

where *FoM* is Figure of Merit, RE_M is the RE for one landscape metric, w_{FoM} is the relative weight of the Figure of Merit, and w_L is the weight for landscape metrics. Only four landscape metrics (AREA_MN, NP, AI, and ED) were used in the calculation of error; CA was excluded because the *f* value does not affect the area of each LULC class in LandScaleR, and the differences in CA between the downscaled and HILDA+ maps were expected to be very small. LandScaleR aims to generate realistic landscape patterns instead of high cell-based accuracy,[44] so we weighted landscape metrics more highly in the calculation of DE. The weight for the figure of merit, w_{FoM}, was set to 0.2, while w_L was set to 0.8, meaning each pattern metric was given equal weight with the figure of merit. The combined DE metric was averaged across the ten repeats for each year to generate a yearly mean DE for all *f* values tested during calibration. Total DE (DE_T) was also calculated by summing DE across all years in the study period for each replicate and then taking an average across replicates to get the country-scale DE_T. Note that we use DE to refer to downscaling error in a single year and DE_T to refer to the total DE between 2010 and 2020. The optimum *f* value for each country was the one with the lowest DE_T value. The maximum possible DE in a single year was 100, and the maximum possible DE_T across the 10-year calibration period was 1,000. The optimum *f* value for the globe was selected by averaging the yearly DE across all country groups and choosing the value that minimized the sum of the yearly DE over time.

Downscaling future LULC projections from LandSyMM

Future LULC projections from LandSyMM[36] were downscaled between 2021 and 2100 using the calibrated LandScaleR model to generate yearly LULC maps with a 0.01° spatial resolution (approximately 1 × 1 km at the equator). Future projections of LULC change from LandSyMM were downscaled for five SSP scenarios, which are narratives of possible future socioeconomic changes.[48–50] Each SSP was paired with an RCP climate scenario that describes an associated climate change under a given trajectory of socioeconomic development.[51] The five scenarios were SSP1-RCP2.6, the "sustainability" scenario; SSP2-RCP4.5, the "middle-of-the-road" scenario; SSP3-RCP7.0, the "regional rivalry" scenario with high climate change; SSP4-RCP6.0, the "inequality" scenario; and SSP5-RCP8.5, the "fossil-fueled development" scenario.[49] For each scenario, a range of parameters can be used in LandSyMM to represent more or less extreme outcomes. The median parameter set for each scenario was selected for downscaling to give

Please cite this article in press as: Woodman et al., High-resolution land-use maps from 1960 to 2100, One Earth (2025), https://doi.org/10.1016/j.oneear.2025.101525

Table 1. Relationship of LandSyMM land-use and land-cover classes to HILDA+ classes

	HILDA+ LULC classes							
LandSyMM LULC classes	Urban	Cropland	Pasture/rangeland	Managed forest	Unmanaged forest	Unmanaged grass/shrubland	Sparse/no vegetation	Water
Urban	1	0	0	0	0	0	0	0
Cropland	0	1	0	0	0	0	0	0
Pasture	0	0	1	0	0	0	0	0
Timber forest	0	0	0	1	0	0	0	0
Unmanaged forest	0	0	0	0	1	0	0	0
Other natural	0	0	0	0	0	ON_g	ON_s	0
Barren	0	0	0	0	0	0	0	1

These relationships were used in LandScaleR to map LULC change from LandSyMM[36] onto HILDA+ LULC classes.[43] ON_g is the coarse-resolution grid-cell-specific proportion of other natural land cover from LandSyMM matched to the unmanaged grass/shrubland HILDA+ class. ON_s is the grid-cell-specific proportion of other natural land cover matched to the sparse/no vegetation class. ON_g and ON_s are dynamically determined for each coarse-resolution 0.5°-resolution grid cell from LandSyMM during each timestep of the downscaling process.

a representative projection. Downscaling was performed twice for each scenario: once where each country was downscaled with its optimum *f* value and second with a single, global-scale *f* value.

HILDA+ LULC in 2020[43] was used as the reference map for downscaling future LULC projections from LandSyMM to ensure that the future projections were harmonized as far as possible with the historic LULC data. Downscaling was performed as for the LandScaleR calibration, with each country downscaled separately before merging all downscaled country-scale maps to generate global downscaled projections. A few countries, such as Greenland, are not modeled in LandSyMM but do have LULC data in HILDA+. Therefore, the downscaled maps were overlaid with the HILDA+ LULC data in 2020 for countries that do not undergo LULC change in LandSyMM so that the high-resolution future LULC projections include the same countries as the historic HILDA+ maps. The kernel density radius parameter in LandScaleR was set to 1.

LandScaleR matches the LULC classes in the coarse-resolution input maps to those in the fine-resolution reference map,[44] so we matched the LandSyMM LULC classes to those in HILDA+, as in Table 1. All LandSyMM LULC classes were matched to a single HILDA+ class except for "other natural" land, which was matched to both unmanaged grass/shrubland and sparse/no vegetation in HILDA+. The proportion of unmanaged grass/shrubland versus sparse/no vegetation cover can vary greatly between countries and within 0.5°-resolution grid cells in HILDA+. Therefore, the proportion of other-natural-land-cover change from LandSyMM assigned to the unmanaged grass/shrubland and sparse/no vegetation classes was determined dynamically within the algorithm for each 0.5°-resolution grid cell based on the proportions of the two LULC classes within that cell in the reference map for that timestep:

$$ON_G = \frac{c_G}{c_G + c_S} \quad \text{and} \qquad \text{(Equation 4)}$$

$$ON_S = \frac{c_S}{c_G + c_S}, \qquad \text{(Equation 5)}$$

where ON_G is the proportion of other natural land cover from LandSyMM assigned to the unmanaged grass/shrubland HILDA+ class, ON_S is the proportion of other natural land cover assigned to the sparse/no vegetation class, c_G is the area of unmanaged grass/shrubland within a 0.5° grid cell from LandSyMM that has been overlaid on the reference map, and c_S is the area of sparse/no vegetation in the reference map within a 0.5°-resolution grid cell from LandSyMM.

RESOURCE AVAILABILITY

Lead contact

Requests for further information and resources should be directed to and will be fulfilled by the lead contact, Tamsin L. Woodman (tamsin.woodman@ed.ac.uk).

Materials availability

This study did not generate new unique materials.

Data and code availability

- The global-scale harmonized LULC dataset generated in this study, which incorporates HILDA+ v.2b and downscaled future LULC projections, is available via Zenodo (Zenodo: https://doi.org/10.5281/zenodo.15017066) along with the LandSyMM model land-cover output data.
- This paper uses global maps of country administrative boundaries that are accessible through the GADM (https://gadm.org/).
- The LandScaleR downscaling algorithm code is openly accessible via GitHub (https://github.com/TamsinWoodman/LandScaleR) under the GNU General Public License v.3.0.
- All original code and the release version of LandScaleR (v.1.1.1) on which this study is based have been archived on Zenodo (Zenodo: https://doi.org/10.5281/zenodo.15067983).
- The LandSyMM model code is publicly accessible via GitLab (https://git.ecdf.ed.ac.uk/lul/plumv2/-/tags/DownscalingPaper).
- Any additional information required to reanalyze the data reported in this paper is available from the lead contact upon request.

ACKNOWLEDGMENTS

T.L.W. was funded by EASTBIO UKRI BBSRC grant number BB/T00875X/1. T.L.W., B.A., and P.A. were supported by the UKRI projects "Co-designing holistic forest-based policy pathways for climate change mitigation" (ForestPaths, 10039590) and "Joined-up land use strategies tackling climate

change and biodiversity loss" (Mosaic, 10075849). R.H. and D.B. acknowledge the generous support of alumni and friends in establishing the University of Aberdeen's Interdisciplinary Institute, which enabled this research, including Dr. Jane Hellman Caseley (MBChB 1956), Professor Patrick Meares (DSc 1959), Nancy Miller (MA 1942), Norman Robertson, Dr. Ian Slessor (MBChB 1956), and Anne Young (MA 1957). All downscaling simulations and calculations of accuracy metrics were performed using the University of Aberdeen HPC, Maxwell.

AUTHOR CONTRIBUTIONS

T.L.W., P.A., J.M.J.T., and D.F.R.P.B. conceptualized the project. B.A. and K.W. provided data for modeling. B.A. contributed code for data preparation. T.L.W. carried out all data preparation, modeling, and analysis. T.L.W. wrote the manuscript with support from J.M.J.T. T.L.W., B.A., K.W., R.C.H., F.E., D.F.R.P.B., P.A., and J.M.J.T. reviewed and edited the manuscript.

DECLARATION OF INTERESTS

The authors declare no competing interests.

DECLARATION OF GENERATIVE AI AND AI-ASSISTED TECHNOLOGIES IN THE WRITING PROCESS

During the preparation of this work, the authors used ChatGPT 4.0 in order to assist in improving the readability of the work. After using this tool/service, the authors reviewed and edited the content as needed and take full responsibility for the content of the publication.

SUPPLEMENTAL INFORMATION

Supplemental information can be found online at https://doi.org/10.1016/j.oneear.2025.101525.

Received: May 1, 2025
Revised: August 19, 2025
Accepted: November 5, 2025

REFERENCES

1. Forzieri, G., Alkama, R., Miralles, D.G., and Cescatti, A. (2017). Satellites reveal contrasting responses of regional climate to the widespread greening of Earth. Science *356*, 1180–1184. https://doi.org/10.1126/science.aal1727.
2. Jaureguiberry, P., Titeux, N., Wiemers, M., Bowler, D.E., Coscieme, L., Golden, A.S., Guerra, C.A., Jacob, U., Takahashi, Y., Settele, J., et al. (2022). The direct drivers of recent global anthropogenic biodiversity loss. Sci. Adv. *8*, eabm9982. https://doi.org/10.1126/sciadv.abm9982.
3. Newbold, T., Hudson, L.N., Hill, S.L.L., Contu, S., Lysenko, I., Senior, R.A., Börger, L., Bennett, D.J., Choimes, A., Collen, B., et al. (2015). Global effects of land use on local terrestrial biodiversity. Nature *520*, 45–50. https://doi.org/10.1038/nature14324.
4. Meier, R., Schwaab, J., Seneviratne, S.I., Sprenger, M., Lewis, E., and Davin, E.L. (2021). Empirical estimate of forestation-induced precipitation changes in Europe. Nat. Geosci. *14*, 473–478. https://doi.org/10.1038/s41561-021-00773-6.
5. Rigby, A.M.F., Butcher, P.W.S., Ritsos, P.D., and Patil, S.D. (2022). LUCST: A novel toolkit for Land Use Land Cover change assessment in SWAT+ to support flood management decisions. Environ. Model. Softw. *156*, 105469. https://doi.org/10.1016/j.envsoft.2022.105469.
6. Arneth, A., Denton, F., Agus, F., Elbehri, A., Erb, K., Osman Elasha, B., Rahimi, M., Rounsevell, M., Spence, A., and Valentini, R. (2019). Framing and Context. In Climate Change and Land, P.R. Shukla, J. Skea, E. Calvo Buendia, V. Masson-Delmotte, H.-O. Pörtner, D.C. Roberts, P. Zhai, R. Slade, S. Connors, R. van Diemen, and M. Ferrat, et al., eds. (Cambridge University Press). https://doi.org/10.1017/9781009157988.003.
7. Luyssaert, S., Jammet, M., Stoy, P.C., Estel, S., Pongratz, J., Ceschia, E., Churkina, G., Don, A., Erb, K., Ferlicoq, M., et al. (2014). Land management and land-cover change have impacts of similar magnitude on surface temperature. Nat. Clim. Chang. *4*, 389–393. https://doi.org/10.1038/nclimate2196.
8. Foley, J.A., Ramankutty, N., Brauman, K.A., Cassidy, E.S., Gerber, J.S., Johnston, M., Mueller, N.D., O'Connell, C., Ray, D.K., West, P.C., et al. (2011). Solutions for a cultivated planet. Nature *478*, 337–342. https://doi.org/10.1038/nature10452.
9. Tilman, D., Balzer, C., Hill, J., and Befort, B.L. (2011). Global food demand and the sustainable intensification of agriculture. Proc. Natl. Acad. Sci. USA *108*, 20260–20264. https://doi.org/10.1073/pnas.1116437108.
10. Haddad, N.M., Brudvig, L.A., Clobert, J., Davies, K.F., Gonzalez, A., Holt, R.D., Lovejoy, T.E., Sexton, J.O., Austin, M.P., Collins, C.D., et al. (2015). Habitat fragmentation and its lasting impact on Earth's ecosystems. Sci. Adv. *1*, e1500052. https://doi.org/10.1126/sciadv.1500052.
11. Jacobson, A.P., Riggio, J., M Tait, A., and E M Baillie, J. (2019). Global areas of low human impact ('Low Impact Areas') and fragmentation of the natural world. Sci. Rep. *9*, 14179. https://doi.org/10.1038/s41598-019-50558-6.
12. Brinck, K., Fischer, R., Groeneveld, J., Lehmann, S., Dantas De Paula, M., Pütz, S., Sexton, J.O., Song, D., and Huth, A. (2017). High resolution analysis of tropical forest fragmentation and its impact on the global carbon cycle. Nat. Commun. *8*, 14855. https://doi.org/10.1038/ncomms14855.
13. World Economic Forum (2024). The Global Risks Report 2024 (World Economic Forum).
14. Pais, C., Miranda, A., Carrasco, J., and Shen, Z.-J.M. (2021). Deep fire topology: Understanding the role of landscape spatial patterns in wildfire occurrence using artificial intelligence. Environ. Model. Softw. *143*, 105122. https://doi.org/10.1016/j.envsoft.2021.105122.
15. Ryu, S.-R., Chen, J., Zheng, D., and Lacroix, J.J. (2007). Relating surface fire spread to landscape structure: An application of FARSITE in a managed forest landscape. Landsc. Urban Plan. *83*, 275–283. https://doi.org/10.1016/j.landurbplan.2007.05.002.
16. Amiri, B.J., Junfeng, G., Fohrer, N., Mueller, F., and Adamowski, J. (2018). Regionalizing Flood Magnitudes using Landscape Structural Patterns of Catchments. Water. Resour. Manage. *32*, 2385–2403. https://doi.org/10.1007/s11269-018-1935-3.
17. Fischer, J., and Lindenmayer, D.B. (2007). Landscape modification and habitat fragmentation: a synthesis. Glob. Ecol. Biogeogr. *16*, 265–280. https://doi.org/10.1111/j.1466-8238.2007.00287.x.
18. Turner, M.G., and Gardner, R.H. (2015). Causes of Landscape Pattern. In Landscape Ecology in Theory and Practice (Springer), pp. 33–62. https://doi.org/10.1007/978-1-4939-2794-4_2.
19. Woodman, T.L., Alexander, P., Burslem, D.F.R.P., Travis, J.M.J., Winkler, K., and Eigenbrod, F. (2025). Global assessment of landscape pattern changes from 1992 to 2020. Landsc. Ecol. *40*, 196. https://doi.org/10.1007/s10980-025-02210-0.
20. Arima, E.Y., Walker, R.T., Perz, S., and Souza, C., Jr (2015). Explaining the fragmentation in the Brazilian Amazonian forest. J. Land Use Sci. *11*, 1–21. https://doi.org/10.1080/1747423X.2015.1027797.
21. Ewers, R.M., and Laurance, W.F. (2006). Scale-dependent patterns of deforestation in the Brazilian Amazon. Environ. Conserv. *33*, 203–211. https://doi.org/10.1017/S0376892906003250.
22. Johnson, J.A., Baldos, U.L., Corong, E., Hertel, T., Polasky, S., Cervigni, R., Roxburgh, T., Ruta, G., Salemi, C., and Thakrar, S. (2023). Investing in nature can improve equity and economic returns. Proc. Natl. Acad. Sci. USA *120*, e2220401120. https://doi.org/10.1073/pnas.2220401120.
23. Chen, G., Li, X., and Liu, X. (2022). Global land projection based on plant functional types with a 1-km resolution under socio-climatic scenarios. Sci. Data *9*, 125. https://doi.org/10.1038/s41597-022-01208-6.

24. Cao, M., Zhu, Y., Quan, J., Zhou, S., Lü, G., Chen, M., and Huang, M. (2019). Spatial sequential modeling and predication of global land use and land cover changes by integrating a global change assessment model and cellular automata. Earths Future *7*, 1102–1116. https://doi.org/10.1029/2019EF001228.

25. Chen, M., Vernon, C.R., Graham, N.T., Hejazi, M., Huang, M., Cheng, Y., and Calvin, K. (2020). Global land use for 2015–2100 at 0.05° resolution under diverse socioeconomic and climate scenarios. Sci. Data *7*, 320. https://doi.org/10.1038/s41597-020-00669-x.

26. Johnson, J.A., Ruta, G., Baldos, U., Cervigni, R., Chonabayashi, S., Corong, E., Gavryliuk, O., Gerber, J., Hertel, T., Nootenboom, C., et al. (2021). The Economic Case for Nature (The World Bank).

27. Li, X., Chen, G., Liu, X., Liang, X., Wang, S., Chen, Y., Pei, F., and Xu, X. (2017). A New Global Land-Use and Land-Cover Change Product at a 1-km Resolution for 2010 to 2100 Based on Human–Environment Interactions. Ann. Am. Assoc. Geogr. *107*, 1040–1059. https://doi.org/10.1080/24694452.2017.1303357.

28. von Jeetze, P.J., Weindl, I., Johnson, J.A., Borrelli, P., Panagos, P., Molina Bacca, E.J., Karstens, K., Humpenöder, F., Dietrich, J.P., Minoli, S., et al. (2023). Projected landscape-scale repercussions of global action for climate and biodiversity protection. Nat. Commun. *14*, 2515. https://doi.org/10.1038/s41467-023-38043-1.

29. Zeng, L., Liu, X., Li, W., Ou, J., Cai, Y., Chen, G., Li, M., Li, G., Zhang, H., and Xu, X. (2022). Global simulation of fine resolution land use/cover change and estimation of aboveground biomass carbon under the shared socioeconomic pathways. J. Environ. Manage. *312*, 114943. https://doi.org/10.1016/j.jenvman.2022.114943.

30. Zhang, T., Cheng, C., and Wu, X. (2023). Mapping the spatial heterogeneity of global land use and land cover from 2020 to 2100 at a 1 km resolution. Sci. Data *10*, 748. https://doi.org/10.1038/s41597-023-02637-7.

31. van Vuuren, D.P., Smith, S.J., and Riahi, K. (2010). Downscaling socioeconomic and emissions scenarios for global environmental change research: a review. Wiley Interdiscip. Rev. Clim. Change *1*, 393–404. https://doi.org/10.1002/wcc.50.

32. Bocedi, G., Palmer, S.C.F., Malchow, A., Zurell, D., Watts, K., and Travis, J.M.J. (2021). RangeShifter 2.0: an extended and enhanced platform for modelling spatial eco-evolutionary dynamics and species' responses to environmental changes. Ecography *44*, 1453–1462. https://doi.org/10.1111/ecog.05687.

33. Titeux, N., Henle, K., Mihoub, J.B., Regos, A., Geijzendorffer, I.R., Cramer, W., Verburg, P.H., and Brotons, L. (2016). Biodiversity scenarios neglect future land-use changes. Glob. Chang. Biol. *22*, 2505–2515. https://doi.org/10.1111/gcb.13272.

34. de Chazal, J., and Rounsevell, M.D.A. (2009). Land-use and climate change within assessments of biodiversity change: A review. Glob. Environ. Change *19*, 306–315. https://doi.org/10.1016/j.gloenvcha.2008.09.007.

35. Hurtt, G.C., Chini, L., Sahajpal, R., Frolking, S., Bodirsky, B.L., Calvin, K., Doelman, J.C., Fisk, J., Fujimori, S., Klein Goldewijk, K., et al. (2020). Harmonization of global land use change and management for the period 850–2100 (LUH2) for CMIP6. Geosci. Model Dev. (GMD) *13*, 5425–5464. https://doi.org/10.5194/gmd-13-5425-2020.

36. Rabin, S.S., Alexander, P., Henry, R., Anthoni, P., Pugh, T.A.M., Rounsevell, M., and Arneth, A. (2020). Impacts of future agricultural change on ecosystem service indicators. Earth Syst. Dyn. *11*, 357–376. https://doi.org/10.5194/esd-11-357-2020.

37. Pereira, H.M., Martins, I.S., Rosa, I.M.D., Kim, H., Leadley, P., Popp, A., van Vuuren, D.P., Hurtt, G., Quoss, L., Arneth, A., et al. (2024). Global trends and scenarios for terrestrial biodiversity and ecosystem services from 1900 to 2050. Science *384*, 458–465. https://doi.org/10.1126/science.adn3441.

38. Borrelli, P., Robinson, D.A., Panagos, P., Lugato, E., Yang, J.E., Alewell, C., Wuepper, D., Montanarella, L., and Ballabio, C. (2020). Land use and climate change impacts on global soil erosion by water (2015-2070). Proc. Natl. Acad. Sci. USA *117*, 21994–22001. https://doi.org/10.1073/pnas.2001403117.

39. Spinoni, J., Barbosa, P., Cherlet, M., Forzieri, G., McCormick, N., Naumann, G., Vogt, J.V., and Dosio, A. (2021). How will the progressive global increase of arid areas affect population and land-use in the 21st century? Glob. Planet. Change *205*, 103597. https://doi.org/10.1016/j.gloplacha.2021.103597.

40. Bocedi, G., Pe'er, G., Heikkinen, R.K., Matsinos, Y., and Travis, J.M.J. (2012). Projecting species' range expansion dynamics: sources of systematic biases when scaling up patterns and processes. Methods Ecol. Evol. *3*, 1008–1018. https://doi.org/10.1111/j.2041-210X.2012.00235.x.

41. Suh, S., Johnson, J.A., Tambjerg, L., Sim, S., Broeckx-Smith, S., Reyes, W., and Chaplin-Kramer, R. (2020). Closing yield gap is crucial to avoid potential surge in global carbon emissions. Glob. Environ. Change *63*, 102100. https://doi.org/10.1016/j.gloenvcha.2020.102100.

42. Alexander, P., Prestele, R., Verburg, P.H., Arneth, A., Baranzelli, C., Batista e Silva, F., Brown, C., Butler, A., Calvin, K., Dendoncker, N., et al. (2017). Assessing uncertainties in land cover projections. Glob. Chang. Biol. *23*, 767–781. https://doi.org/10.1111/gcb.13447.

43. Winkler, K., Fuchs, R., Rounsevell, M.D.A., and Herold, M. (2025). HILDA+ Version 2.0: Global Land Use Change between 1960 and 2020 (PANGAEA). https://doi.pangaea.de/10.1594/PANGAEA.974335.

44. Woodman, T.L., Rueda-Uribe, C., Henry, R.C., Burslem, D.F.R.P., Travis, J.M.J., and Alexander, P. (2023). Introducing LandScaleR: A novel method for spatial downscaling of land use projections. Environ. Model. Softw. *169*, 105826. https://doi.org/10.1016/j.envsoft.2023.105826.

45. Paegelow, M., Mas, J.-F., Gallardo, M., Camacho Olmedo, M.T., and García-Álvarez, D. (2022). Pontius Jr. Methods Based on a Cross-Tabulation Matrix to Validate Land Use Cover Maps. In Land Use Cover Datasets and Validation Tools: Validation Practices with QGIS (Springer International Publishing), pp. 153–187. https://doi.org/10.1007/978-3-030-90998-7.

46. Pontius, R.G., Boersma, W., Castella, J.-C., Clarke, K., de Nijs, T., Dietzel, C., Duan, Z., Fotsing, E., Goldstein, N., Kok, K., et al. (2008). Comparing the input, output, and validation maps for several models of land change. Ann. Reg. Sci. *42*, 11–37. https://doi.org/10.1007/s00168-007-0138-2.

47. Hesselbarth, M.H.K., Sciaini, M., With, K.A., Wiegand, K., and Nowosad, J. (2019). landscapemetrics: an open-source R tool to calculate landscape metrics. Ecography *42*, 1648–1657. https://doi.org/10.1111/ecog.04617.

48. O'Neill, B.C., Carter, T.R., Ebi, K., Harrison, P.A., Kemp-Benedict, E., Kok, K., Kriegler, E., Preston, B.L., Riahi, K., Sillmann, J., et al. (2020). Achievements and needs for the climate change scenario framework. Nat. Clim. Chang. *10*, 1074–1084. https://doi.org/10.1038/s41558-020-00952-0.

49. O'Neill, B.C., Kriegler, E., Ebi, K.L., Kemp-Benedict, E., Riahi, K., Rothman, D.S., van Ruijven, B.J., van Vuuren, D.P., Birkmann, J., Kok, K., et al. (2017). The roads ahead: Narratives for shared socioeconomic pathways describing world futures in the 21st century. Glob. Environ. Change *42*, 169–180. https://doi.org/10.1016/j.gloenvcha.2015.01.004.

50. O'Neill, B.C., Kriegler, E., Riahi, K., Ebi, K.L., Hallegatte, S., Carter, T.R., Mathur, R., and van Vuuren, D.P. (2014). A new scenario framework for climate change research: the concept of shared socioeconomic pathways. Clim. Change *122*, 387–400. https://doi.org/10.1007/s10584-013-0905-2.

51. van Vuuren, D.P., Edmonds, J., Kainuma, M., Riahi, K., Thomson, A., Hibbard, K., Hurtt, G.C., Kram, T., Krey, V., Lamarque, J.-F., et al. (2011). The representative concentration pathways: an overview. Clim. Change *109*, 5–31. https://doi.org/10.1007/s10584-011-0148-z.

52. Alexander, P., Rabin, S., Anthoni, P., Henry, R., Pugh, T.A.M., Rounsevell, M.D.A., and Arneth, A. (2018). Adaptation of global land use and management intensity to changes in climate and atmospheric carbon dioxide. Glob. Chang. Biol. *24*, 2791–2809. https://doi.org/10.1111/gcb.14110.

53. Smith, B., Wårlind, D., Arneth, A., Hickler, T., Leadley, P., Siltberg, J., and Zaehle, S. (2014). Implications of incorporating N cycling and N limitations on primary production in an individual-based dynamic

vegetation model. Biogeosciences *11*, 2027–2054. https://doi.org/10.5194/bg-11-2027-2014.

54. Chen, G., Li, X., Liu, X., Chen, Y., Liang, X., Leng, J., Xu, X., Liao, W., Qiu, Y., Wu, Q., and Huang, K. (2020). Global projections of future urban land expansion under shared socioeconomic pathways. Nat. Commun. *11*, 537. https://doi.org/10.1038/s41467-020-14386-x.

55. Cattarino, L., McAlpine, C.A., and Rhodes, J.R. (2014). Land-use drivers of forest fragmentation vary with spatial scale. Glob. Ecol. Biogeogr. *23*, 1215–1224. https://doi.org/10.1111/geb.12187.

56. Romanillos, G., Robazza, G., and Lovato, F. (2024). A fragmented world: mapping the global extent of Anthropogenic Landscape Fragmentation. J. Maps *20*, 2307539. https://doi.org/10.1080/17445647.2024.2307539.

57. Fahrig, L. (2003). Effects of Habitat Fragmentation on Biodiversity. Annu. Rev. Ecol. Evol. Syst. *34*, 487–515. https://doi.org/10.1146/annurev.ecolsys.34.011802.132419.

58. Fletcher, R.J., Jr., Reichert, B.E., and Holmes, K. (2018). The negative effects of habitat fragmentation operate at the scale of dispersal. Ecology *99*, 2176–2186. https://doi.org/10.1002/ecy.2467.

59. Arnold, J.G., Srinivasan, R., Muttiah, R.S., and Williams, J.R. (1998). LARGE AREA HYDROLOGIC MODELING AND ASSESSMENT PART I: MODEL DEVELOPMENT[1]. J. Am. Water Resour. Assoc. *34*, 73–89. https://doi.org/10.1111/j.1752-1688.1998.tb05961.x.

60. Bieger, K., Arnold, J.G., Rathjens, H., White, M.J., Bosch, D.D., Allen, P.M., Volk, M., and Srinivasan, R. (2017). Introduction to SWAT +, A Completely Restructured Version of the Soil and Water Assessment Tool. J. American Water Resour. Assoc. *53*, 115–130. https://doi.org/10.1111/1752-1688.12482.

61. Abbaspour, K.C., Rouholahnejad, E., Vaghefi, S., Srinivasan, R., Yang, H., and Kløve, B. (2015). A continental-scale hydrology and water quality model for Europe: Calibration and uncertainty of a high-resolution large-scale SWAT model. J. Hydrol. X. *524*, 733–752. https://doi.org/10.1016/j.jhydrol.2015.03.027.

62. Volpato, M., Andrade, C.F., Silva, E.L., Barbosa, M.L., Andrade, M.D., Rocha, P.V., Delgado, R.C., Teodoro, P.E., Silva, C.A., and Pereira, M.G. (2023). Fire foci and their spatiotemporal relations to weather variables and land uses in the state of Mato Grosso. Environ. Dev. Sustain. *25*, 12419–12438. https://doi.org/10.1007/s10668-022-02573-3.

63. Kumar, S., Getirana, A., Libonati, R., Hain, C., Mahanama, S., and Andela, N. (2022). Changes in land use enhance the sensitivity of tropical ecosystems to fire-climate extremes. Sci. Rep. *12*, 964. https://doi.org/10.1038/s41598-022-05130-0.

64. Finney, M.A. (1998). FARSITE: Fire Area Simulator-Model Development and Evaluation (U.S. Department of Agriculture, Forest Service, Rocky Mountain Research Station). https://doi.org/10.2737/RMRS-RP-4.

65. Parisien, M.A., Kafka, V.G., Hirsch, K.G., Todd, J.B., Lavoie, S.G., and Maczek, P.D. (2005). MAPPING WILDFIRE SUSCEPTIBILITY WITH THE BURN-P3 SIMULATION MODEL (Canadian Forest Service).

66. Natural Capital Project (2025). InVEST 3.16.1. Stanford University, University of Minnesota, Chinese Academy of Sciences (The Nature Conservancy, World Wildlife Fund, Stockholm Resilience Centre and the Royal Swedish Academy of Sciences). https://doi.org/10.60793/natcap-invest-3.16.1.

67. Mukhopadhyay, A., Hati, J.P., Acharyya, R., Pal, I., Tuladhar, N., and Habel, M. (2025). Global trends in using the InVEST model suite and related research: A systematic review. Ecohydrol. Hydrobiol. *25*, 389–405. https://doi.org/10.1016/j.ecohyd.2024.06.002.

68. Fallert, S., Li, L., and Cabral, J.S. (2025). metaRange: A framework to build mechanistic range models. Methods Ecol. Evol. *16*, 49–56. https://doi.org/10.1111/2041-210X.14461.

69. Montti, L., Palmer, S.C.F., Powell, P.A., Burslem, D.F.R.P., Travis, J.M.J., and Ponchon, A. (2025). Modelling alternative management strategies of invasive tree species at the expansion front: *Ligustrum lucidum* as a case study. Ecol. Sol. and Evidence *6*, e70012. https://doi.org/10.1002/2688-8319.70012.

70. Winkler, K., Fuchs, R., Rounsevell, M., and Herold, M. (2021). Global land use changes are four times greater than previously estimated. Nat. Commun. *12*, 2501–2510. https://doi.org/10.1038/s41467-021-22702-2.

71. Winkler, K., Fuchs, R., Rounsevell, M.D.A., and Herold, M. (2020). HILDA+ Global Land Use Change between 1960 and 2019 (PANGAEA). https://doi.org/10.1594/PANGAEA.921846.

72. R Core Team (2022). R: A Language and Environment for Statistical Computing (R Foundation for Statistical Computing). https://www.R-project.org/.(RFoundationforStatisticalComputing.

73. Hijmans, R.J. (2022). terra: Spatial Data Analysis. R package version *1*, 7–23. https://rspatial.org/terra/.

74. University of California, Berkeley (2018). Database of Global Administrative Boundaries (GADM) [dataset]. Version 3.6. https://gadm.org.VersionVersion3.6 https://gadm.org.

75. Hijmans, R.J., Barbosa, M., Ghosh, A., and Mandel, A. (2023). geodata: Download Geographic Data. R package version 0.5-9. https://CRAN.R-project.org/package=geodata.

76. Dezhkam, S., Jabbarian Amiri, B., Darvishsefat, A.A., and Sakieh, Y. (2016). Performance evaluation of land change simulation models using landscape metrics. Geocarto Int. *32*, 1–23. https://doi.org/10.1080/10106049.2016.1167967.

77. Li, X., Lin, J., Chen, Y., Liu, X., and Ai, B. (2013). Calibrating cellular automata based on landscape metrics by using genetic algorithms. Int. J. Geogr. Inf. Sci. *27*, 594–613. https://doi.org/10.1080/13658816.2012.698391.

78. Lin, J., Li, X., Li, S., and Wen, Y. (2020). What is the influence of landscape metric selection on the calibration of land-use/cover simulation models? Environ. Model. Softw. *129*, 104719. https://doi.org/10.1016/j.envsoft.2020.104719.